Synthesis and Dynamic NMR Studies of η^3-Triphenyl- and η^3-Trimethylcyclopropenyl Complexes of Ruthenium, $[Ru(\eta^5\text{-}C_5R_5)(\eta^3\text{-}C_3R'_3)X_2]$ (R = H, Me; R′ = Me, Ph; X = Cl, Br, I). Extended Hückel Molecular Orbital Study of Barriers to Rotation of η^3-Cyclopropenyl Ligands in Isoelectronic Ruthenium and Molybdenum Complexes

Robert Ditchfield,* Russell P. Hughes,* David S. Tucker, Erik P. Bierwagen, Jennifer Robbins, David J. Robinson, and Julie A. Zakutansky

Department of Chemistry, Burke Laboratory, Dartmouth College, Hanover, New Hampshire 03755

Received December 22, 1992

Oxidative addition reactions of triphenylcyclopropenyl halides to Ru(II) precursors $[Ru(\eta^5\text{-}C_5H_5)(\eta^4\text{-COD})Cl]$ and $[Ru(\eta^5\text{-}C_5Me_5)Cl]_4$ afford $[Ru(\eta^5\text{-}C_5R_5)(\eta^3\text{-}C_3Ph_3)Cl_2]$ (**3a**, R = H; **3e**, R = Me). Derivative complexes $[Ru(\eta^5\text{-}C_5R_5)(\eta^3\text{-}C_3Ph_3)X_2]$ (**3b** R = H, X = Br; **3c** R = H, X = I; **3f** R = Me, X = Br; **3g** R = Me, X = I) were prepared by halide metathesis reactions on **3a** and **3e**. Solution NMR evidence for the mixed halide complex $[Ru(\eta^5\text{-}C_5H_5)(\eta^3\text{-}C_3Ph_3)BrCl]$ (**3d**) has also been obtained. Rotation of the triphenylcyclopropenyl ring about the Ru–C_3 axis in **3** is not observable on the NMR time scale. Similar reactions of trimethylcyclopropenyl tetrafluoroborate with the same Ru(II) precursors, in the presence of lithium chloride, lead to $[Ru(\eta^5\text{-}C_5R_5)(\eta^3\text{-}C_3Me_3)Cl_2]$ (**4a**, R = H; **4d**, R = Me), which were converted to the dibromo and diiodo analogues $[Ru(\eta^5\text{-}C_5R_5)(\eta^3\text{-}C_3Me_3)X_2]$ (**4b** R = H, X = Br; **4c** R = H, X = I; **4e** R = Me, X = Br; **4f** R = Me, X = I) by halide metathesis. The ^1H NMR spectra of complexes **4** exhibit variable temperature behavior, consistent with rotation of the trimethylcyclopropenyl ligand on the NMR time scale. Line shape analysis of the variable temperature spectra leads to values for the free energy of activation ($\Delta G^{\ddagger}$) for this rotation of ca. 60 kJ mol^{-1}, which are insensitive to the nature of the halide or the cyclopentadienyl ligand. These relatively high values of $\Delta G^{\ddagger}$ stand in contrast to the maximum value of $\Delta G^{\ddagger}$ for triphenylcyclopropenyl rotation estimated previously for an isoelectronic complex $[Mo(\eta^5\text{-}C_5H_5)(\eta^3\text{-}C_3Ph_3)(CO)_2]$ (**2**). A detailed theoretical analysis at the extended Hückel level has been carried out for the bonding interactions between both $[Ru(\eta^5\text{-}C_5H_5)Br_2]$ and $[Mo(\eta^5\text{-}C_5H_5)(CO)_2]$ fragments and the $[C_3H_3]$ ligand. This analysis predicts a significantly higher barrier to cyclopropenyl rotation in the Ru system and provides a rational picture of the electronic structural features which give rise to the observed differences in values of $\Delta G^{\ddagger}$ for cyclopropenyl rotation in the two systems.

Introduction

The dynamic behavior of η^2-olefin complexes of the transition metals has been the subject of extensive investigation for the past three decades, and a large body of experimental data exists on the activation energy barriers for propeller rotation of ligated olefins.[1] The factors which influence the relative magnitudes of these activation barriers have been probed by application of a fragment molecular orbital approach at the extended Hückel level to the transition metal unit responsible for binding the olefin ligand. This approach, coupled with the powerful isolobal analogy, has allowed a detailed theoretical understanding of this important form of dynamic behavior to be achieved.[2]

Far less information is available on the dynamic behavior of the η^3-cyclopropenyl ligand, partly because the range of available complexes of this ligand is small. Transition metal complexes of this ligand are important because of the metallacyclobutadiene/η^3-cyclopropenyl valence isomeric relationship, and its possible importance in alkyne metathesis continues to stimulate considerable interest.[3] The activation barrier to rotation of the cyclopropenyl ligand about the M–C_3 axis has been shown to vary dramatically with the nature of the metal–ligand fragment, and attempts have been made to correlate the presence or absence of this behavior with structural features pertaining to the M–C_3 interaction. For example, in the formally d^2 W(IV) complex **1** the cyclopropenyl ring is

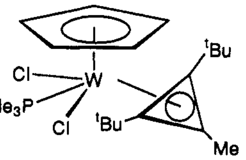

1

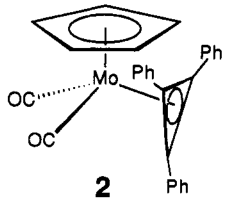

2

conformationally rigid on the NMR time scale in solution

(1) A compendium of such activation barriers appears in: Mann, B. L. In *Comprehensive Organometallic Chemistry*; Wilkinson, G., Abel, E., Stone, F. G. A., Eds.; Pergamon: Oxford, U.K., 1983; Vol. 3, Chapter 20, p 89.

(2) For recent treatments of this bonding model see: (a) Albright, T. A.; Hoffman, R.; Thibeault, J. C.; Thorn, D. L. *J. Am. Chem. Soc.* 1979, *101*, 3801. (b) Mingos, D. M. P. *Comprehensive Organometallic Chemistry*; Wilkinson, G., Abel, E., Stone, F. G. A., Eds.; Pergamon: Oxford, U.K., 1983; Vol. 3, Chapter 19, p 1.

(3) Schrock, R. R. *Acc. Chem. Res.* 1986, *19*, 342 and references therein.

0276-7333/93/2312-2258$04.00/0

at ambient temperature, and the solid state structure shows a distance from the metal to the C_3 ring centroid (1.991 Å) shorter than that to the C_5 ring centroid (2.046 Å).[4] Contrasting behavior is exhibited by the formally d^4 Mo(II) complex **2**, in which the cyclopropenyl ring rotates rapidly on the NMR time scale at −80 °C and whose solid state structure exhibits a distance to the C_5 centroid (1.997 Å) shorter than that to the C_3 centroid (2.055 Å).[5] While compounds **1** and **2** were the closest analogues available for structural and spectroscopic comparison, it was not clear whether the difference in formal d-electron configuration between the metals, steric effects due to different coordination numbers at the metal or different ring substituents, and/or the apparently tighter binding of the C_3 ring in complex **1** was responsible for the difference in rotational barriers between **1** and **2**. Subsequent synthesis and characterization of the cyclopropenyl–ruthenium complexes **3** clouded the issue even further. The cyclo-

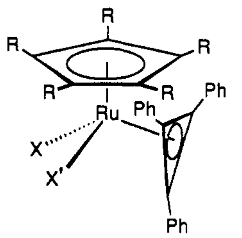

3a R = H; X = X' = Cl
3b R = H; X = X' = Br
3c R = H; X = X' = I
3d R = H; X = Cl; X' = Br
3e R = Me; X = X' = Cl
3f R = Me; X = X' = Br
3g R = Me; X = X' = I

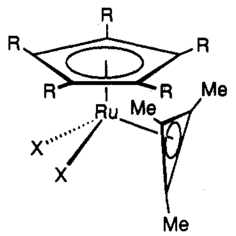

4a R = H; X = Cl
4b R = H; X = Br
4c R = H; X = I
4d R = Me; X = Cl
4e R = Me; X = Br
4f R = Me; X = I

propenyl ligands in **3** were conformationally rigid on the NMR time scale, yet the molecular structure of **3b** was virtually isostructural with that of **2**, demonstrating a clear lack of correlation between structural factors or steric effects and the barrier to cyclopropenyl rotation.[6] Clearly, while both the $[RuCpBr_2]$ and $[MoCp(CO)_2]$ fragments are isolobal with CH, it is the detailed nature of their bonding interactions with the C_3 ring which must govern the relative magnitude of ΔG^* for cyclopropenyl rotation.

Unfortunately, the presence or absence of cyclopropenyl rotation in complexes **1–3** is absolute on the NMR time scale, and only estimates of ΔG^* for cyclopropenyl rotation could be obtained.[6] Thus, complexes **3** were nonfluxional at room temperature, as evidenced by the observation of two inequivalent cyclopropenyl ring carbon resonances in the ^{13}C NMR spectrum. The smallest separation between inequivalent cyclopropenyl ring carbon resonances was observed to be 30 Hz in the mixed halide complex **3d**, and the coalescence temperature is clearly >298 K. The equation $\Delta G^*_{coalescence} = 0.01914T_{coalescence}[9.972 + \log(T_c/\Delta\nu)]$ leads to an estimated *minimum* ΔG^* for cyclopropenyl rotation of 62 kJ mol^{-1} for this complex.[6] Complex **2** was fluxional even at −193 K; only a single resonance for the cyclopropenyl ring carbon atoms was observed at this temperature.[5] The assumption that $\Delta\nu$ for **2** was the same as the $\Delta\delta$ for the inequivalent cyclopropenyl ^{13}C resonances observed for **3a** (3000 Hz) and the knowledge that the coalescence temperature was <−193 K led to an estimated *maximum* value for ΔG^* of 32 kJ mol^{-1} for **2**.[6]

Prior to the work reported in this paper, no activation parameters for such cyclopropenyl rotation had been measured experimentally. Here we report the first examples of cyclopropenyl complexes that exhibit variable temperature NMR behavior consistent with such rotation and that allow experimental measurement of the activation barriers for this process. We also report a theoretical study at the extended Hückel level that provides a clear explanation of why the barriers to such rotation should be considerably higher for cyclopropenyl ligands bound to the $[RuCpBr_2]$ fragment as compared to the isoelectronic $[MoCp(CO)_2]$ moiety.

Results and Discussion

Synthesis and Characterization. Oxidative addition reactions of allylic halides to the ruthenium(II) fragment $[Ru(\eta^5\text{-}C_5H_5)X]$, obtained by displacement of 1,5-cyclooctadiene (COD) from $[Ru(\eta^5\text{-}C_5H_5)(\eta^4\text{-}COD)X]$ (X = Cl, Br),[7] are known to give η^3-allylic complexes of Ru(IV).[8] Prior to this work, analogous oxidative addition reactions with the respective triphenylcyclopropenyl halide salts had been shown to proceed at room temperature in methanol solution to give good yields of the red-orange, air stable, crystalline complexes **3a** and **3b**.[6] The halide ligands are substitutionally labile; metathetical reactions of a methanol solution of **3a** with sodium bromide or potassium iodide yield **3b** and **3c**, while treatment of $[Ru(\eta^5\text{-}C_5H_5)(\eta^4\text{-}COD)Cl]$ with triphenylcyclopropenyl bromide affords a mixture of **3a**, **3b**, and the mixed halide complex **3d**. The corresponding pentamethylcyclopentadienyl (Cp*) analogue **3e** was prepared by reaction of the tetramer, $[Ru(\eta^5\text{-}C_5Me_5)Cl]_4$,[9] with triphenylcyclopropenyl chloride in THF. To complete the series of triphenylcyclopropenyl complexes, the bromo and iodo analogues **3f** and **3g** were prepared by metathetical reaction of solutions of **3e** with LiX (X = Br, I), or more effectively with aqueous HX (X = Br, I).

The molecular structure of dibromo complex **3b** has been determined by a single crystal X-ray diffraction study, that shows the ground state structure of the complex to be that depicted in the line drawing, with one edge of the cyclopropenyl ring lying parallel to the plane of the Cp ring and the unique cyclopropenyl carbon atom pointing away from the Cp ring.[6] NMR spectroscopic analysis of all complexes **3** indicated that the solid state structure is maintained in solution. The presence of two ^{13}C resonances for the cyclopropenyl ring carbon atoms and

(4) Churchill, M. R.; Fettinger, J. C.; McCullough, L.; Schrock, R. R. *J. Am. Chem. Soc.* **1984**, *106*, 3356.
(5) Hughes, R. P.; Reisch, J. W.; Rheingold, A. L. *Organometallics* **1985**, *4*, 1754 and references therein.
(6) Hughes, R. P.; Robbins, J.; Robinson, D. J.; Rheingold, A. L. *Organometallics* **1988**, *7*, 2413.
(7) (a) Albers, M. O.; Oosthuizen, H. E.; Robinson, D. J.; Shaver, A.; Singleton, E. *J. Organomet. Chem.* **1985**, *282*, C49. (b) Albers, M. O.; Robinson, D. J.; Shaver, A.; Singleton, E. *Organometallics* **1986**, *5*, 2199.
(8) (a) Albers, M. O.; Liles, D. C.; Robinson, D. J.; Shaver, A.; Singleton, E. *J. Chem. Soc., Chem. Commun.* **1986**, 645. (b) Albers, M. O.; Liles, D. C.; Robinson, D. J.; Shaver, A.; Singleton, E. *Organometallics* **1987**, *6*, 2347. (c) Nagashima, H.; Mukai, K.; Itoh, K. *Organometallics* **1984**, *3*, 1314. (d) Nagashima, H.; Mukai, K.; Shiota, Y.; Ara, K.; Itoh, K.; Suzuki, H.; Oshima, N.; Moro-oka, Y. *Organometallics* **1985**, *4*, 1314. (e) Nagashima, H.; Mukai, K.; Shiota, Y.; Yamaguchi, K.; Ara, K.; Fukahori, T.; Suzuki, H.; Akita, M.; Moro-oka, Y.; Itoh, K. *Organometallics* **1990**, *9*, 799.
(9) (a) Fagan, P. J.; Ward, M. D.; Calabrese, J. C. *J. Am. Chem. Soc.* **1989**, *111*, 1698. (b) Fagan, P. J.; Ward, M. D.; Caspar, J. V.; Calabrese, J. C.; Krusic, P. J. *J. Am. Chem. Soc.* **1988**, *110*, 2981. (c) Koelle, U.; Kossakowski, J. *J. Chem. Soc., Chem. Commun.* **1988**, 549.

resonances due to two different phenyl groups indicates a conformationally static structure in solution on the NMR time scale. The observation of three cyclopropenyl ring carbon resonances for the mixed halo complex **3d** is also consistent with conformational rigidity.

The preparation of trimethylcyclopropenyl analogues **4** was possible using similar methodology. Unlike the triphenylcyclopropenyl cation, which can be isolated as its halide salts,[10] the corresponding trimethylcyclopropenyl cation is most easily prepared as its BF_4^- salt.[11] However, this salt reacted readily with THF solutions of [Ru(η^5-C_5H_5)(η^4-COD)Cl], or [Ru(η^5-C_5Me_5)Cl]$_4$ in the presence of LiCl, to afford the C_3Me_3 complexes **4a** and **4d**. In turn these compounds underwent metathetical halide replacement with HBr or HI, to afford the corresponding compounds **4b,c,e,f**. These compounds were characterized by NMR spectroscopy and microanalysis.

It was not possible to separate complex **4f** from a persistent impurity, even after chromatography and many recrystallizations. The impurity exhibited a singlet at δ 1.68 in the ^{1}H NMR spectrum. The possibility that the peak at δ 1.68 represents the mixed halide [RuCp*(η^3-C_3Me_3)(Cl)I] was contemplated. However, when 1 equiv of hydriodic acid was added to a $CDCl_3$ solution of **4a** in an NMR tube, the Cp* peak at δ 1.62 (**4a**) decreased, with the appearance of resonances at δ 1.68, 1.80, and 1.97 (**4f**). Subsequent addition of excess hydriodic acid to this sample resulted in decreased intensities of the peaks at δ 1.62 (**4a**) and δ 1.80. Thus the δ 1.80 peak is assigned to the mixed halide complex. It is possible that the impurity giving rise to the δ 1.68 peak is that of [RuCp*I]$_4$ (^{1}H NMR (THF-d_8) δ 1.69).[12]

In contrast to their triphenyl analogues **3**, compounds **4** exhibited variable temperature NMR behavior. At low temperatures, two ^{1}H NMR resonances were observed for the methyl groups of the cyclopropenyl ring. On warming, these resonances coalesced and subsequently sharpened to a single peak with a chemical shift at the weighted average of the original two methyl environments. Cooling reversed the process, which is consistent with rotation of the trimethylcyclopropenyl ring on the NMR time scale. These are the first observations of such variable temperature behavior in a cyclopropenyl complex. The low temperature ^{13}C{^{1}H} NMR spectra of complexes **4** also showed two resonances of relative intensity 2:1 for the cyclopropenyl ring carbons and for the cyclopropenyl methyl groups, but no attempts were made to explore the dynamics of the system using variable temperature ^{13}C NMR spectra.

It is noteworthy that comparison of complexes containing Cp (**4a–c**) with those containing Cp* (**4d–f**), under conditions of slow exchange, reveals that the changes in chemical shift between the two frozen out methyl resonances of the trimethylcyclopropenyl ring are consistent with the proposed ground state structure. A change from Cp to Cp* ligands has a perturbing effect that is stronger on the ^{1}H resonance of the two equivalent methyls than on that of the unique methyl; e.g., for **4a** and **4d** the resonance for the equivalent methyl groups differs by 0.28 ppm while that for the unique methyl changes by only 0.02 ppm. Similar effects are noted for analogous pairs **4b**/**4d** and **4c**/**4f**. In contrast, changing the halogen ligands has a perturbing effect that is stronger on the resonance of the unique methyl group than on the resonance associated with the equivalent methyls. Comparison of the dichloride **4a** to the diiodide **4c** shows that the resonance due to the equivalent methyls changes by only 0.03 ppm while that of the unique methyl changes by 0.45 ppm. Assuming that changing ligands most strongly affects the chemical shifts of those methyl substituents situated in closest proximity, these observations support the illustrated structure as that of the ground state in solution at low temperature. The unique methyl lies closer to the halogens, while the equivalent methyls lie closer to the C_5 ring. Attempts to use NOE difference measurements to provide further evidence were inconclusive.

Table I. $\Delta G^{\ddagger}$ Values for Rotation about the Ru–C_3 Axis in Complexes 4

complex	$\Delta G^{\ddagger}$ (298 K) (kJ mol^{-1})^a
[RuCp(C_3Me_3)Cl_2] (**4a**)	59.6 ± 1.6
[RuCp(C_3Me_3)Br_2] (**4b**)	62.5 ± 1.4
[RuCp(C_3Me_3)I_2] (**4c**)	64.5 ± 1.7
[RuCp*(C_3Me_3)Cl_2] (**4d**)	58.4 ± 1.6
[RuCp*(C_3Me_3)Br_2] (**4e**)	60.6 ± 1.0
[RuCp*(C_3Me_3)I_2] (**4f**)	61.7 ± 1.5

^{a} Measured in $CDCl_3$ solution.

Experimental Measurement of $\Delta G^{\ddagger}$ for Trimethylcyclopropenyl Rotation Using NMR Line Shape Analysis. The NMR line shape of the signals due to the cyclopropenyl methyl groups was easily modeled with a three site exchange process with two symmetry equivalent and one unique methyl environment.[13] Simulation of the observed spectra afforded rate constants at various temperatures, and free energies of activation were then obtained via the Eyring equation which provides $\Delta G^{\ddagger}$ from a weighted least squares plot of k/T vs $e^{-1/T}$.

Table I shows the experimentally obtained barriers to cyclopropenyl rotation for the complexes **4a–f**. These experimental data reveal a remarkable lack of sensitivity of $\Delta G^{\ddagger}$ to changes in the cyclopentadienyl ring or halide substituents. The steric bulk of the C_5 ligand appears to have no effect on the relative values of $\Delta G^{\ddagger}$. A comparison of Cp complexes to their respective Cp* complexes, e.g., **4a** to **4d**, shows no change in $\Delta G^{\ddagger}$ within experimental error. Similarly, changing the halogens has only a small effect on $\Delta G^{\ddagger}$, and an apparent increase in $\Delta G^{\ddagger}$ as the larger halogens are used is still within experimental error. Notably, these experimentally measured values of $\Delta G^{\ddagger}$ are virtually identical to the estimated minimum value of $\Delta G^{\ddagger} \geq 62$ kJ mol^{-1} for the triphenyl analogue **3d**.[6]

With some firm experimental numbers now in place, we turn now to the question of why the value of $\Delta G^{\ddagger}$ for internal rotation of a cyclopropenyl ligand bound to a $RuCpX_2$ fragment should be so much higher than that for the corresponding isoelectronic $MoCp(CO)_2$ complex.

Theoretical Studies

The problem we consider is the origin of the barrier to internal rotation of the η^3-C_3R_3 ligand in molecules **2** and **3**/**4**. We will rationalize the observed equilibrium con-

(10) Breslow, R.; Chang, H. W. *J. Am. Chem. Soc.* **1961**, *83*, 2367.
(11) Closs, G. L.; Böll, W. A.; Heyn, H.; Dev, V. *J. Am. Chem. Soc.* **1968**, *90*, 173.
(12) Fagan, P. J.; Mahoney, J. C.; Calabrese, J. C.; Williams, I. D. *Organometallics* **1990**, *9*, 1843.

(13) The original version of the dynamic NMR simulation program was written by: Kleier, D. A.; Binsch, G. *J. Magn. Reson.* **1970**, *3*, 146–160; Program 165, Quantum Chemistry Program Exchange, Indiana University. Modifications are described in: Bushweller, C. H.; Bhat, G.; Lentendre, L. J.; Brunelle, J. A.; Bilofsky, H. S.; Ruben, H.; Templeton, D. H.; Zalkin, A. *J. Am. Chem. Soc.* **1975**, *97*, 65–73.

Table II. Parameters Used in the Extended Hückel Calculations

orbital		H_{ii} (eV)	ζ_1	ζ_2	C_1[a]	C_2[a]
C	2s	−21.40	1.625			
	2p	−11.40	1.625			
O	2s	−32.30	2.275			
	2p	−14.80	2.275			
H	1s	−13.60	1.30			
Br	4s	−22.07	2.588			
	4p	−13.10	2.130			
Mo	5s	−8.41	1.96			
	5p	−5.28	1.90			
	4d	−11.04	4.54	1.90	0.6097	0.6097
R	5s	−8.39	2.08			
	5p	−4.97	2.04			
	4d	−12.47	5.38	2.30	0.5342	0.6368

[a] Coefficients in the double ζ expansion.

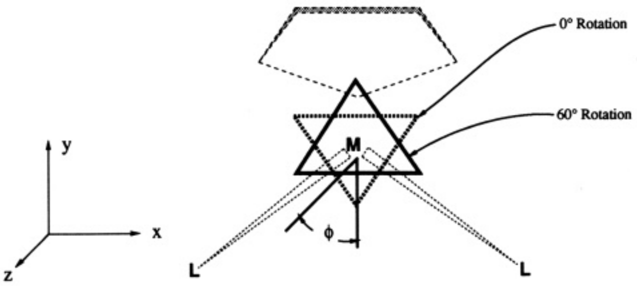

Figure 1. Definition of the rotational angle ϕ used in the extended Hückel analysis.

formations and the barriers to rotation in these complexes using the results of extended Hückel calculations on the model complexes [$MoCp(CO)_2(\eta^3\text{-}C_3H_3)$] and [$RuCpBr_2(\eta^3\text{-}C_3H_3)$]. In particular, our analysis will identify the interactions which make important contributions to the barrier to internal rotation in such systems. A comparison of these interactions in [$MoCp(CO)_2(\eta^3\text{-}C_3H_3)$] with those in [$RuCpBr_2(\eta^3\text{-}C_3H_3)$] will provide a rationalization of the larger barrier height in the latter.

The first step in this theoretical study was to calculate the barrier to internal rotation of the $\eta^3\text{-}C_3H_3$ ligand in [$MoCp(CO)_2(\eta^3\text{-}C_3H_3)$] and [$RuCpBr_2(\eta^3\text{-}C_3H_3)$]. The extended Hückel method[14,15] was used with parameters specified in Table II. The internal rotation coordinate ϕ is defined in Figure 1; all other bond lengths and angles were held fixed at the values specified in Appendix A (supplementary material). Figure 2 shows a plot of the potential energy barriers to rotation of C_3H_3 in [$MoCp(CO)_2(\eta^3\text{-}C_3H_3)$] and [$RuCpBr_2(\eta^3\text{-}C_3H_3)$]. These results indicate that, for both molecules, the most stable conformation is that with $\phi = 0°$, in agreement with the conformations observed in the crystal structures of [$MoCp(CO)_2(\eta^3\text{-}C_3Ph_3)$][5] and [$RuCpBr_2(\eta^3\text{-}C_3Ph_3)$].[6] In both cases, the unique carbon of the cyclopropenyl moiety points away from the cyclopentadienyl ring. In addition, the extended Hückel method calculates a larger barrier to rotation in the ruthenium complex, in qualitative agreement with the experimental data reported above.

The molecular orbitals (MOs) of [$MCpL_2(\eta^3\text{-}C_3H_3)$] can be obtained in a number of ways. In the present case, we take as a framework for the analysis of these rotational barriers the conceptual construction of the complex from [$MCpL_2$] and [C_3H_3] fragments. The MOs of the [$MCpL_2$] fragments are first developed and then allowed to interact with the orbitals of [C_3H_3] in extreme geometries that correspond to the minima and maxima of the rotational potential energy function. The MOs of [$MCpL_2$] are constructed by considering interaction of the orbitals of the [MCp] fragment with those of the L_2 ligands. Detailed discussions of the metal-containing frontier orbitals of [MCp] have been given by Lauher et al.[16] Here we describe only those orbitals which are important in understanding the differences in the rotational barriers of the molybdenum and ruthenium complexes.

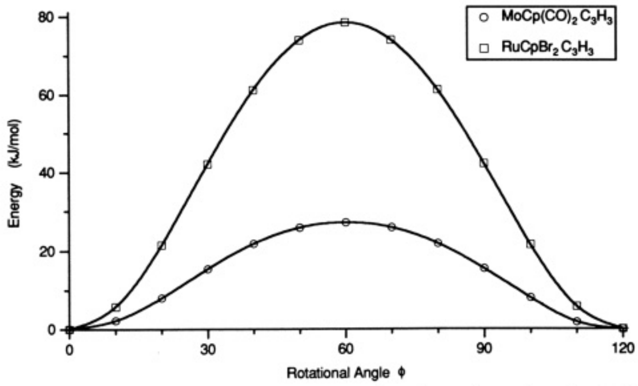

Figure 2. Plot of energy vs rotational angle ϕ for the [$\eta^3\text{-}C_3H_3$] ring in [$MoCp(CO)_2(C_3H_3)$] and [$RuCpBr_2(C_3H_3)$].

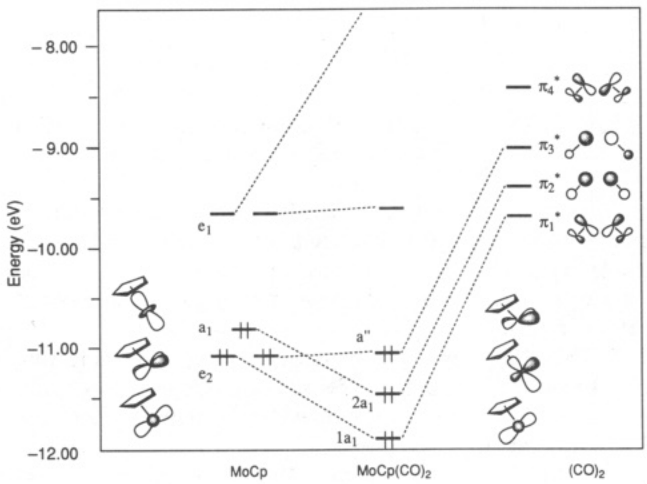

Figure 3. Interaction of the frontier orbitals of the [MoCp] fragment with the π MOs of two CO ligands.

Interaction of the metal atom d-orbitals with the π-type MOs of the cyclopentadienyl ring splits the 5-fold degeneracy of the metal d-orbitals into σ (a_1), π (e_1), and δ (e_2) sets. As shown in the left hand columns of Figures 3 and 4, the e_2 MOs containing the two d-orbitals involved in a weak δ bonding interaction with higher-lying π^* MOs of the Cp ring are the lowest lying. The e_1 MOs containing the two d-orbitals involved in a strong π^* antibonding interaction with lower-lying π^* MOs of the Cp ring are the highest lying, while the a_1 MO containing a single d-orbital involved in a σ^* antibonding interaction with the lowest-lying π MO of the Cp ring has an energy intermediate between the δ and π^* sets. As our subsequent analysis will show, the nature and the behavior of the lower-lying δ- and σ^*-type MOs play an important role in understanding the rotational barriers in the molybdenum and ruthenium cyclopropenyl complexes.

The calculations performed here indicate that the relative ordering and the shapes of the metal-containing MOs of [MoCp] and [RuCp] are qualitatively quite similar,

(14) Hoffmann, R. *J. Chem. Phys.* **1963**, *39*, 1397. Hoffmann, R.; Lipscomb, W. N. *Ibid.* **1962**, *36*, 2179, 3489; **1962**, *37*, 2872.
(15) Ammeter, J. H.; Bürgi, H.-B.; Thibeault, J. C.; Hoffmann, R. *J. Am. Chem. Soc.* **1978**, *100*, 3686.

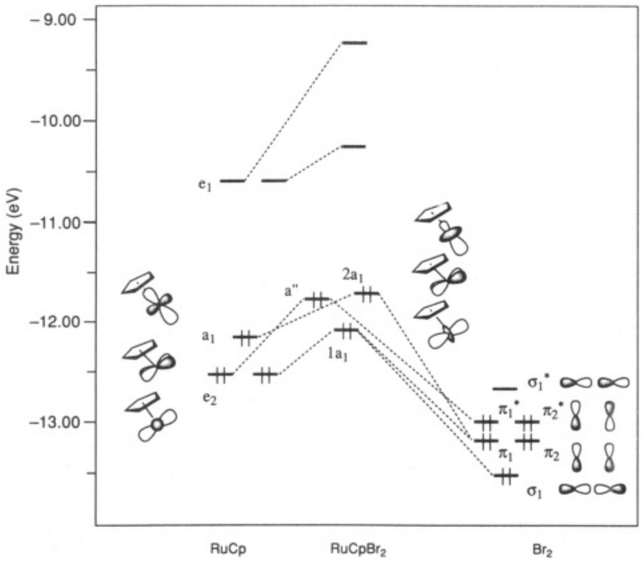

Figure 4. Interaction of the frontier orbitals of the [RuCp] fragment with the σ and π MOs of two Br ligands.

in agreement with studies on the [MCp] fragment reported by Lauher et al.[16] We note that the MOs for [RuCp] are lower in energy, associated with the lower energy d-orbitals on Ru, and that the e_2–a_1 MO energy gap is somewhat larger in [RuCp].

MCpL$_2$ Fragments. With a qualitative understanding of the electronic structure of the [MCp] fragment in hand, the next step is to examine how the L_2 ligands affect the MCp orbitals described above.

[MoCp(CO)$_2$] Fragment. As shown in the central column of Figure 3, the addition of CO ligands splits the degeneracy of the e_2 level; the $1a_1$ component is stabilized considerably, while the energy of the a″ MO remains essentially unchanged. The a_1 MO of [MoCp] is also substantially lowered on interaction with the CO ligands. For [MoCp(CO)$_2$] these changes arise almost totally from an interaction of the [MoCp] orbitals with the carbonyl vacant π^* MOs. This is in marked contrast to results reported[17] for carbonyl complexes of first-row metals where interactions with carbonyl σ MOs play an important role in determining the energies, shapes, and orientations of the MOs for [MCpL$_2$]. Replacing a first-row metal with molybdenum raises the energy of the free-atom d-orbitals with the result that the MOs of the [MoCp] fragment are much closer in energy to the carbonyl vacant π^* MOs. Since the interaction of the $1a_1$, $2a_1$, and a″ orbitals with those of the cyclopropenyl fragment play the dominant role in rationalizing the rotational barrier, the shapes of these MOs are analyzed in some detail.

We begin with the a″ orbital. The carbonyl π_3^* orbital has an overall stronger bonding interaction with the d_{xz} component of the e_2 orbital than with the d_{xy} component (see **5**). This has the effect of increasing the contribution of the d_{xz} component in a″ relative to that of the d_{xy} component, with the result that the a″ MO tilts considerably toward the xz-plane. In addition, the metal p_x orbital mixes in such a way as to increase further the

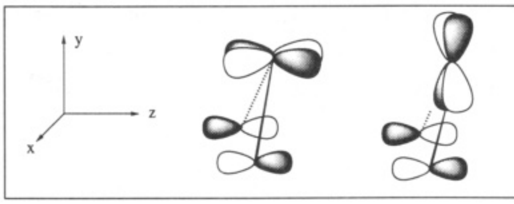

5

bonding character. The net effect, shown in **6**, is to

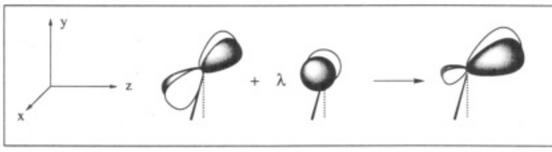

6

hybridize the metal orbital away from the attached carbonyls and towards the incoming cyclopropenyl ring. Both these changes produce a decrease in the bonding interaction of the metal with the Cp ring with the net result that the energy of the a″ shows little change on addition of the CO ligands. As already noted above, in contrast to the case of [FeCp(CO)$_2$], the a″ orbital has very little interaction with the carbonyl σ-orbitals.

The $2a_1$ orbital also has little interaction with the carbonyl σ-orbitals. In this case the main interaction is with the carbonyl π_2^* orbital which has an overall stronger bonding interaction with the d_{yz} component of the a_1 orbital than with the $d_{x^2-y^2}$ component. This has the effect of increasing the contribution of the d_{yz} component in $2a_1$ relative to that of the $d_{x^2-y^2}$ component. In addition, the metal p_y orbital mixes in such a way as to increase further the bonding character. The net effect, shown in **7**, is, again,

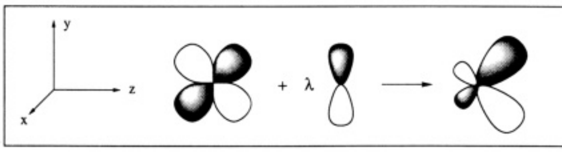

7

to hybridize the metal orbital away from the attached carbonyls and toward the incoming cyclopropenyl ring. Furthermore, these changes reduce the antibonding interaction of the metal with the Cp ring with the net result that the energy of the $2a_1$ orbital is lowered markedly.

The $1a_1$ orbital arises from a bonding interaction of the $d_{x^2-y^2}$, d_{yz}, and d_{z^2} components of the remaining e_2 orbital with the carbonyl π_1^* orbital. In addition, the metal p_z and p_y orbitals interact slightly with the carbonyl π_1^* orbital to increase further the bonding character. Except for a small rehybridization toward the attached carbonyls the shape of this orbital remains largely unchanged. The net result of these bonding interactions is a significant energy lowering.

[RuCpBr$_2$] Fragment. As shown in the central column of Figure 4, the addition of Br ligands splits the degeneracy of the e_2 level. In this case, all three levels of [RuCp] are destabilized by antibonding interactions with the lower-lying filled orbitals of the Br_2 fragment shown. As was found for [MoCp(CO)$_2$(η^3-C_3H_3)], the interactions of the $1a_1$, $2a_1$, and a″ orbitals with those of the cyclopropenyl fragment play the dominant role in rationalizing the rotational barrier in [RuCpBr$_2$(η^3-C_3H_3)].

First, we discuss the nature of the a″ orbital. The Br_2 σ^* and π^* orbitals combine with the higher-lying e_2 orbital in an antibonding fashion. Such interactions are more strongly antibonding with the d_{xy} component of the e_2

(16) Lauher, J. W.; Elian, M.; Summerville, R.; Hoffmann, R. *J. Am. Chem. Soc.* **1976**, *98*, 3219.

(17) See for example: Albright, T. A.; Hofmann, P.; Hoffmann, R. *J. Am. Chem. Soc.* **1977**, *99*, 7546. Thorn, D. L.; Hoffmann, R. *Inorg. Chem.* **1978**, *17*, 126. Schilling, B. E. R.; Hoffmann, R.; Lichtenberger, D. L. *J. Am. Chem. Soc.* **1979**, *101*, 585. Albright, T. A.; Hoffmann, R.; Thibeault, J. C.; Thorn, D. L. *Ibid.* **1979**, *101*, 3801.

orbital than with the d_{xz} component (see **8**). This results

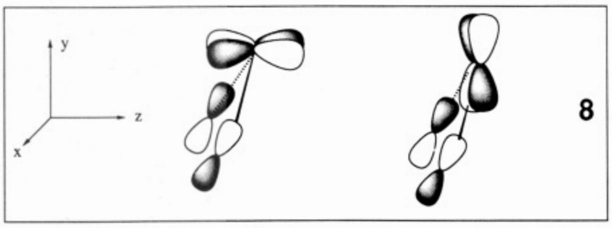

8

in an increase in the magnitude of the d_{xz} component in a″ relative that of the d_{xy} component, with the result that the a″ MO tilts toward the xz-plane. In addition, the metal p_x orbital mixes in to a small extent so as to decrease further the antibonding character. The net effect, shown in **9**, is to produce a slight rehybridization of the metal

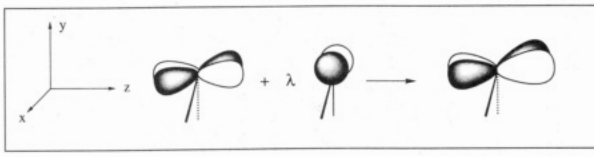

9

orbital away from the attached bromines and toward the incoming cyclopropenyl ring. Both these changes are less pronounced than those found for the a″ orbital in [MoCp(CO)$_2$]; for example, the tilt toward the xz-plane is approximately 50% of that calculated for [MoCp(CO)$_2$]. The net effect of these antibonding interactions is a significant increase in the a″ energy.

The main interaction of the a$_1$ orbital is with the bromine π orbitals. This is antibonding with the larger d_{yz} component of a$_1$, but bonding with the $d_{x^2-y^2}$ component. To reduce the antibonding character of 2a$_1$ in RuCpBr$_2$ the magnitude of the d_{yz} contribution is reduced relative to that of $d_{x^2-y^2}$, and the metal p_y orbital mixes in to a small extent in a bonding fashion. This produces a change in shape and a rehybridization away from the Cp ring, as shown in **10**. The net antibonding result of these interactions raises the energy of 2a$_1$ to approximately the level of a″.

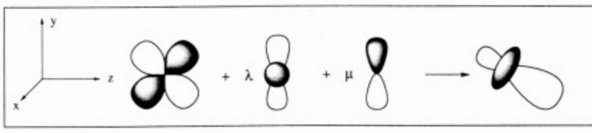

10

The other e$_2$ orbital mixes with the σ and π bromine orbitals. The largest of such antibonding interactions is with the $d_{x^2-y^2}$ component of e$_2$. Thus, to decrease the antibonding character of the 1a$_1$ orbital the magnitude of the $d_{x^2-y^2}$ contribution is reduced relative to those of the d_{yz} and d_{z^2} components, resulting in the change of shape shown in Figure 4.

[MCpL$_2$(η^3-C$_3$H$_3$)] Complexes. The shapes, orientations, and energies of the metal-containing orbitals of the [MCpL$_2$] fragments developed above can now be used to explore the rotational barriers in [MoCp(CO)$_2$(η^3-C$_3$H$_3$)] and [RuCpBr$_2$(η^3-C$_3$H$_3$)]. In each complex the relevant principal orbital interactions are between the 1a$_1$, 2a$_1$, and a″ MOs of [MCpL$_2$] and the π-type (a$_1$ and e) MOs of the cyclopropenyl moiety. We develop MO diagrams for the full complexes by combining the MOs of the appropriate [MCpL$_2$] fragment with those of [C$_3$H$_3$] in extreme geometries that correspond to minima (ϕ = 0°) and maxima (ϕ = 60°) of the rotational potential energy function.

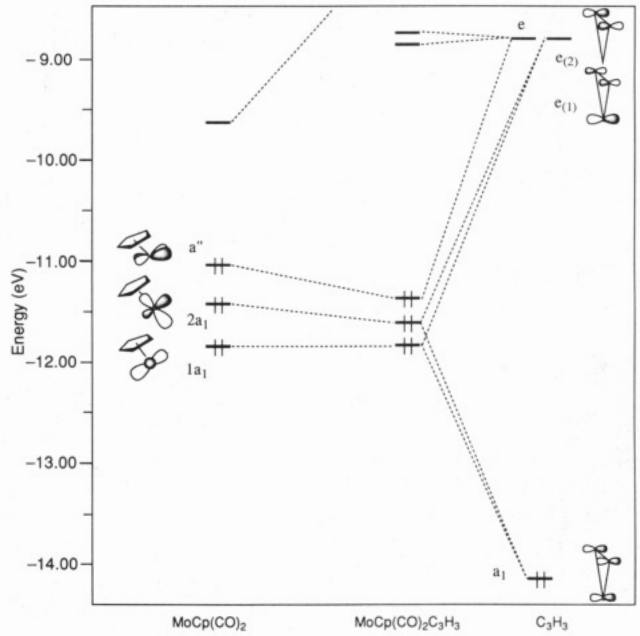

Figure 5. Interaction of the frontier orbitals of [MoCp(CO)$_2$] with those of [C$_3$H$_3$] in the conformation with ϕ = 0°.

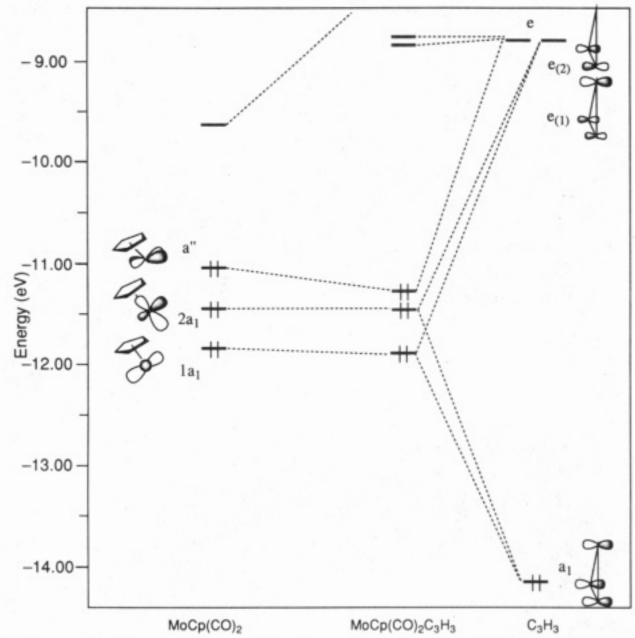

Figure 6. Interaction of the frontier orbitals of [MoCp(CO)$_2$] with those of [C$_3$H$_3$] in the conformation with ϕ = 60°.

Figures 5 and 6 show such MO diagrams for [MoCp(CO)$_2$(η^3-C$_3$H$_3$)] in these two orientations, while Figures 7 and 8 show the corresponding MO interaction diagrams for [RuCpBr$_2$(η^3-C$_3$H$_3$)]. These figures show that, for both types of complex, there are significantly greater bonding interactions between the π-type MOs of [C$_3$H$_3$] and the MOs of [MCpL$_2$] in the ϕ = 0° orientation than in the ϕ = 60° orientation.

We first consider the molybdenum complex. In the ϕ = 0° orientation of [MoCp(CO)$_2$(η^3-C$_3$H$_3$)], the 1a$_1$ MO can combine with the lower energy a$_1$ orbital of [C$_3$H$_3$] in an antibonding sense, and with the higher energy e(1) orbital in a bonding interaction. The rehybridization of the 1a$_1$ orbital in [MoCp(CO)$_2$] reduces the antibonding interaction with the a$_1$ orbital of [C$_3$H$_3$]. In addition, neither the orientation of 1a$_1$ nor the relative contributions of the p_π atomic orbitals in e(1) favor a strong bonding

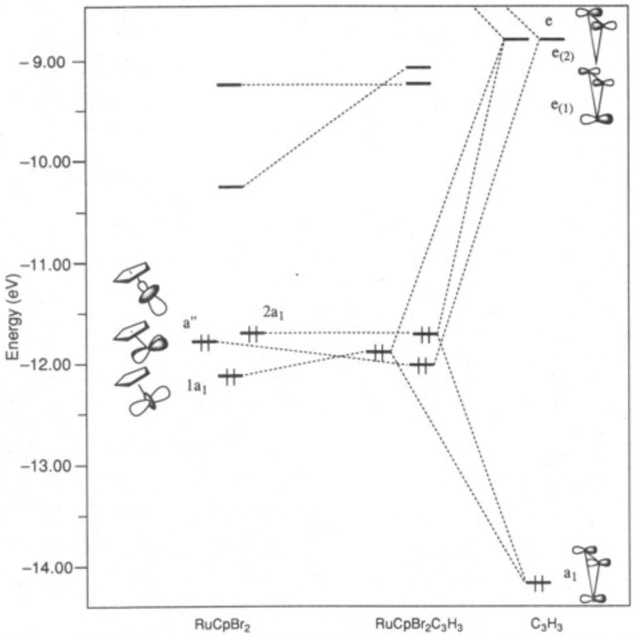

Figure 7. Interaction of the frontier orbitals of [$RuCpBr_2$] with those of [C_3H_3] in the conformation with ϕ = 0°.

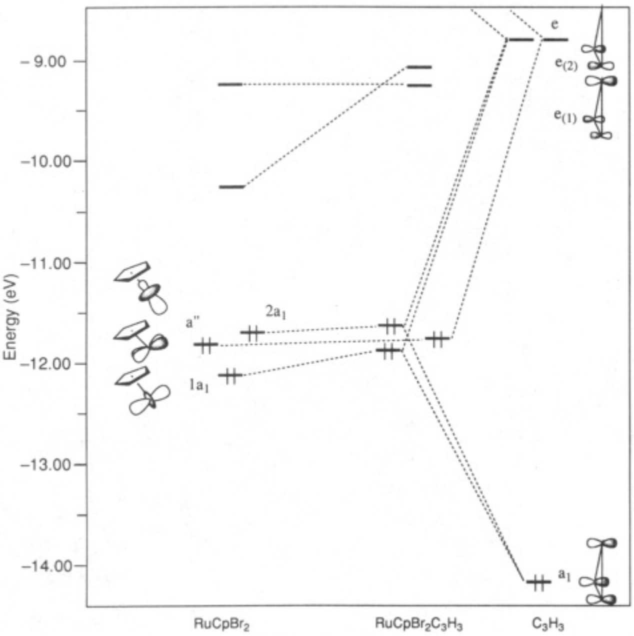

Figure 8. Interaction of the frontier orbitals of [$RuCpBr_2$] with those of [C_3H_3] in the conformation with ϕ = 60°.

interaction. As a result, the energy of the $1a_1$ orbital remains essentially unchanged on addition of [C_3H_3]. The $2a_1$ MO can also combine with the lower energy a_1 orbital of C_3H_3 in a weakly antibonding sense, and with the higher energy e(1) orbital in a much stronger bonding interaction. In this case, the rehybridization of $2a_1$ serves to increase slightly the antibonding interaction with a_1, and to make the bonding interaction with e(1) larger. The $2a_1$–e(1) bonding interaction is dominant and the energy of the $2a_1$ orbital is lowered significantly as the cyclopropenyl fragment is added. The a″ MO can only combine with the e(2) MO of [C_3H_3]. The shape, orientation, and energy of this orbital enable it to participate effectively in a bonding interaction with e(2), and the energy of a″ is reduced as [C_3H_3] is added.

In the ϕ = 60° orientation of [$MoCp(CO)_2(\eta^3\text{-}C_3H_3)$], the a″ is again stabilized significantly on addition of [C_3H_3]

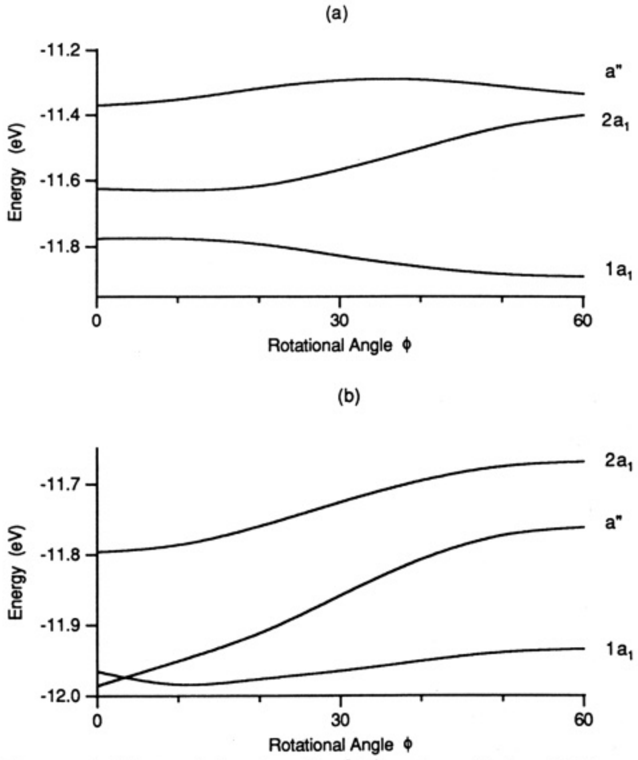

Figure 9. Plots of the energies of the three highest MOs vs the rotational angle ϕ: (a) for [$MoCp(CO)_2(C_3H_3)$]; (b) for [$RuCpBr_2(C_3H_3)$].

but to a somewhat smaller extent than that found when ϕ = 0°. Although the tilt of a″ away from the Cp ring enables this orbital to maintain a bonding interaction with e(2), it is less favorable than in the ϕ = 0° orientation. The energy of the $2a_1$ orbital is now increased slightly since, in this orientation, neither the rehybridization of $2a_1$ nor the relative magnitudes of the p_π atomic orbital contributions to e(1) favor a strong bonding interaction between $2a_1$ and e(1). The $1a_1$ orbital is lowered slightly since the ϕ = 60° orientation now makes the bonding interaction with e(1) more favorable.

Such ideas can be used to rationalize the details of Figure 9a which shows the variations in the a″, $1a_1$, and $2a_1$ orbital energies of [$MoCp(CO)_2(\eta^3\text{-}C_3H_3)$] as ϕ is changed. The a″ orbital energy varies little as ϕ is changed. This is consistent with ability of a″ to combine in a favorable bonding interaction with e(2) at both ϕ = 0° and ϕ = 60°. The rise in the energy of $2a_1$ can be rationalized in terms of the loss of the favorable bonding interaction with e(1) as ϕ increases. The lowering of the $1a_1$ energy can be explained by an increase in the favorable interaction with e(1) as ϕ increases.

As Figure 9a shows, the destabilization of $2a_1$ produced as the [C_3H_3] moiety is rotated is offset to a significant extent by the stabilization of $1a_1$. This leads to a relatively low barrier to rotation of the cyclopropenyl fragment in [$MoCp(CO)_2(\eta^3\text{-}C_3H_3)$].

We now consider the extended Hückel MO analysis for [$RuCpBr_2(\eta^3\text{-}C_3H_3)$]. In the ϕ = 0° orientation, the $1a_1$ MO can combine with the lower energy a_1 orbital of [C_3H_3] in an antibonding sense and with the higher energy e(1) orbital in a bonding interaction. Since the $1a_1$ orbital energy in [$RuCpBr_2$] is lower than that in [$MoCp(CO)_2$] and since the $1a_1$ orbital is not rehybridized toward the bromine ligands, the antibonding interaction with a_1 of [C_3H_3] is significantly greater and the bonding interaction with e(1) is substantially reduced. As a result the energy of the $1a_1$ orbital increases on addition of $[C_3H_3]$. The $2a_1$ MO can also combine with the lower energy a_1 orbital of $[C_3H_3]$ in an antibonding sense and with the higher energy e(1) orbital in a bonding interaction. In this case, both the lower energy of the $1a_1$ orbital and the rehybridization of $2a_1$ away from the Cp ring serve to increase the antibonding interaction with a_1, while maintaining a bonding interaction with e(1). These competing interactions essentially cancel and the energy of the $2a_1$ orbital shows little change as the cyclopropenyl fragment is added. The a″ MO can only combine with the e(2) MO of $[C_3H_3]$. The shape and the orientation of this orbital enable it to participate in a strong bonding interaction with e(2), and the energy of a″ is reduced as $[C_3H_3]$ is added.

In the $\phi = 60°$ orientation of $[RuCpBr_2(\eta^3\text{-}C_3H_3)]$, the energy of the a″ orbital shows essentially no change on addition of $[C_3H_3]$. Since the plane of this orbital is tilted only slightly away from the Cp ring plane, it has little favorable bonding interaction with e(2) in this orientation. As was the case in the $\phi = 0°$ orientation, the antibonding interaction of the $1a_1$ orbital of $[RuCpBr_2]$ with the a_1 orbital of $[C_3H_3]$ is significantly greater than the bonding interaction of $1a_1$ with e(1). As a result the energy of the $1a_1$ orbital increases on addition of $[C_3H_3]$. The energy of the $2a_1$ orbital is also now increased slightly since, in this orientation, both the rehybridization of $2a_1$ and the relative magnitudes of the p_π atomic orbital contributions to e(1) lead to a reduced bonding interaction between $2a_1$ and e(2). In this orientation none of the interactions outlined here are stabilizing.

Such ideas can be used to explain the details of Figure 9b which shows the variations in the a″, $1a_1$, and $2a_1$ orbital energies of $[RuCpBr_2(\eta^3\text{-}C_3H_3)]$ as ϕ is changed. The a″ orbital energy shows a large increase as ϕ is increased. This is consistent with the ability of a″ to participate in a favorable bonding interaction with e(2) at $\phi = 0°$ and with the removal of this stabilizing interaction at $\phi = 60°$. The rise in the energy of $2a_1$ can be rationalized in terms of the loss of the favorable bonding interaction with e(1) as ϕ changes. The $1a_1$ energy shows little change, since neither the antibonding interaction of the $1a_1$ orbital of $[RuCpBr_2]$ with the a_1 orbital of $[C_3H_3]$, nor the bonding interaction of $1a_1$ with e(1) is altered significantly as the $[C_3H_3]$ fragment is rotated.

As Figure 9b shows, the strong destabilization of a″ produced as the $[C_3H_3]$ moiety is rotated is accompanied by a similar contribution from the $2a_1$ orbital. In this case the lack of stabilizing contributions leads to a significantly greater barrier to rotation of the cyclopropenyl fragment in $[RuCpBr_2(\eta^3\text{-}C_3H_3)]$ as compared with the case for $[MoCp(CO)_2(\eta^3\text{-}C_3H_3)]$.

Experimental and Theoretical Procedures

Theoretical Studies. All the calculations reported here were performed using the extended Hückel method[14] with a weighted H_{ij} formula.[15] The H_{ii} parameters and the valence orbital exponents for carbon, oxygen, and hydrogen were taken from the work of Hoffmann et al.[14] The H_{ii}'s for bromine were those proposed by Hinze and Jaffe,[18] while the valence orbital exponents for bromine were from the studies of Clementi and Roetti.[19] The H_{ii}'s for molybdenum and ruthenium were obtained from charge iterative calculations on the lowest structures of $[MoCp(CO)_2(\eta^3\text{-}C_3H_3)]$ and $[RuCpBr_2(\eta^3\text{-}C_3H_3)]$ by assuming a quadratic dependence of metal H_{ii}'s on charge,[20] while the H_{ii} values of all other atoms were kept constant. The iteration parameters were taken from Munita and Letelier.[21] The exponents for the 5s, 5p, and 4d orbitals of molybdenum and ruthenium were taken from the work of Basch and Gray.[22] The values for the H_{ii}'s and orbital exponents are listed in Table II. All computations were carried out with the Chem-X suite of programs developed and distributed by Chemical Design Ltd., Oxford, England.

General Experimental Procedures. Unless otherwise designated, all reactions were performed under a dinitrogen atmosphere using standard Schlenk techniques. The dinitrogen was deoxygenated over BASF catalyst and dried over Aquasorb. All ^1H NMR spectra (300 MHz) and $^{13}C\{^1H\}$ NMR spectra (75 MHz) were obtained on a Varian Associates XL-300 spectrometer at 22 °C unless otherwise noted. Chemical shifts for ^1H spectra and $^{13}C\{^1H\}$ spectra were recorded in ppm downfield from TMS and referenced with internal $CDCl_3$. Variable temperature NMR spectra were recorded on a Varian Associates XL-300 spectrometer. The probe was calibrated at various temperatures by using samples of methanol (low temperature)[23] and ethylene glycol (high temperature).[24] Infrared spectra were recorded on a Bio-Rad Digilab FTS-40 Fourier transform infrared spectrophotometer. All solvents were dinitrogen saturated. Hydrocarbon and ethereal solvents were distilled over potassium or a sodium/potassium alloy. Methylene chloride was distilled over calcium hydride. Melting points were obtained using an Electrothermal capillary melting point apparatus and are uncorrected. Microanalyses were performed by Spang Microanalytical Laboratory, Eagle Harbor, MI.

Starting Materials. Lithium chloride, lithium iodide, hydriodic acid, deuteriochloroform, and naphthalene were purchased from Aldrich Chemical Co. Potassium was purchased from the J. T. Baker Chemical Co. Sodium and hydrobromic acid were purchased from Alfa Chemical Co. Silica gel was obtained from Davison Chemical, Inc. Trimethylphosphine was prepared by a modification of the procedure of Wolfsberger and Schmidbaur.[25] $RuCl_3\cdot xH_2O$ was obtained from Johnson-Matthey Aesar/Alfa.

$[RuCp^*(\mu_3\text{-}Cl)]_4$ was prepared from the polymer $(RuCp^*Cl_2)_n$ by the procedure of Fagan.[9a] $[RuCp(\eta^4\text{-}COD)X]$ (X = Cl, Br) was prepared according to the method of Singleton.[7a] Triphenylcyclopropenyl chloride,[10] bromide,[10] and hexafluorophosphate[5] and trimethylcyclopropenyl tetrafluoroborate[11] were prepared by literature procedures.

(η^5-Cyclopentadienyl)(η^3-triphenylcyclopropenyl)dichlororuthenium(IV) (3a). (a) To methanol (50 mL) was added $[RuCp(\eta^4\text{-}COD)Cl]$ (1.55 g, 5.00 mmol) and triphenylcyclopropenyl chloride (1.50 g, 5.00 mmol). The mixture was allowed to stir for 12 h, after which time an orange-red precipitate had formed. The solid was filtered in air and washed with methanol and diethyl ether (2 × 10 mL each) to yield **3a** (1.7 g, 3.3 mmol, 66%): mp 210–212 °C; ^1H NMR ($CDCl_3$) δ 7.99 (m, br, 4H, Ph), 7.81 (m, br, 2H, Ph), 7.43 (m, br, 6H, Ph), 7.32 (m, br, 3H, Ph), 5.00 (s, 5H, C_5H_5); $^{13}C\{^1H\}$ NMR ($CDCl_3$) δ 134.8, 131.7, 130.0, 129.9, 129.5, 127.4, (Ph), 93.9 (C_5H_5), 93.1 (1C, CPh), 52.8 (2C, CPh). Anal. Calcd for $C_{26}H_{20}Cl_2Ru$: C, 61.91; H, 4.00; Cl, 14.06. Found: C, 61.75; H, 3.81; Cl, 14.48.

(b) To CH_2Cl_2 (15 mL) was added $[RuCp(\eta^4\text{-}COD)Cl]$ (0.16 g, 0.50 mmol) and triphenylcyclopropenyl chloride (0.15 g, 0.50 mmol). The mixture was allowed to stir for 0.5 h, after which time the solution had turned deep orange-red. Solvent and cyclooctadiene were removed under reduced pressure leaving a red-orange solid. The solid was washed with diethyl ether (5 mL), affording **3a** (0.17 g, 0.34 mmol, 68%) (identified by ^1H NMR).

(18) Hinze, J.; Jaffe, H. H. *J. Phys. Chem.* **1963**, *67*, 1501.
(19) Clementi, E.; Roetti, C. *At. Data Nucl. Data Tables* **1974**, *14*, 179.
(20) Basch, H.; Viste, A.; Gray, H. B. *Theor. Chim. Acta* **1965**, *3*, 458.
(21) Munita, R.; Letelier, J. R. *Theor. Chim. Acta* **1981**, *58*, 167.
(22) Basch, H.; Gray, H. B. *Theor. Chim. Acta* **1967**, *4*, 367.
(23) Van Geet, A. L. *Anal. Chem.* **1968**, *40*, 2227–2229.
(24) Van Geet, A. L. *Anal. Chem.* **1970**, *42*, 679–680.
(25) Wolfsberger, W.; Schmidbaur, H. *Synth. React. Inorg. Met.-Org. Chem.* **1974**, *4*, 149.

(c) To CH_2Cl_2 (15 mL) was added [RuCp(η^4-COD)Cl] (0.16 g, 0.50 mmol), triphenylcyclopropenyl hexafluorophosphate (0.21 g, 0.50 mmol), finely crushed potassium chloride (0.37 g, 5.0 mmol), and 18-crown-6 (0.025 mmol, 0.007 g). The mixture was allowed to stir for 24 h, after which time the supernatant solution had turned red. This solution was removed via filter cannula, leaving behind a light brown solid. The solvent was removed from the red solution under reduced pressure, and the product was washed with diethyl ether to yield **3a** (0.15 g, 0.29 mmol, 59%) (identified by ^{1}H NMR).

(d) To acetonitrile (15 mL) was added [RuCp(η^4-COD)Cl] (0.16 g, 0.50 mmol), triphenylcyclopropenyl hexafluorophosphate (0.21 g, 0.50 mmol), and sodium chloride (0.29 g, 5.0 mmol). A color change from brown to deep red occurred within 10 min. After 2 h, a red-orange precipitate was observed. The supernatant solution was removed via filter cannula, and the solid left behind was extracted with CH_2Cl_2. Solvent removal and subsequent washing with diethyl ether yielded **3a** (0.12 g, 0.24 mmol, 48%) (identified by ^{1}H NMR).

(η^5-Cyclopentadienyl)(η^3-triphenylcyclopropenyl)dibromoruthenium(IV) (3b). To methanol (50 mL) was added [RuCp(η^4-COD)Br] (1.77 g, 5.00 mmol) and triphenylcyclopropenyl bromide (1.7 g, 5.0 mmol). The mixture was allowed to stir for 12 h, after which time an orange-red precipitate had formed. The solid was filtered in air and washed with methanol and diethyl ether (2 × 10 mL each) to yield **3b** (1.9 g, 3.2 mmol, 64%): mp 165 °C; ^{1}H NMR ($CDCl_3$) δ 8.08 (m, br, 4H, Ph), 7.92 (m, br, 2H, Ph), 7.51 (m, br, 6H, Ph), 7.40 (m, br, 3H, Ph), 5.17 (s, 5H, C_5H_5); $^{13}C\{^1H\}$ NMR ($CDCl_3$) δ 134.7, 131.7, 130.2, 130.0, 129.5, 129.3, 127.2, 124.6 (Ph), 93.3 (C_5H_5), 89.2 (1C, *C*Ph), 50.3 (2C, *C*Ph). Anal. Calcd for $C_{26}H_{20}Br_2Ru$: C, 52.63; H, 3.40; Br, 26.93. Found: C, 52.42; H, 3.19; Br, 26.77.

(η^5-Cyclopentadienyl)(η^3-triphenylcyclopropenyl)bromochlororuthenium(IV) (3d). To methanol (50 mL) was added [RuCp(η^4-COD)Br] (1.78 g, 5.03 mmol) and triphenylcyclopropenyl chloride (1.7 g, 5.0 mmol). The mixture was allowed to stir for 12 h, after which time an orange-red precipitate had formed. The solid was filtered in air and washed with methanol and diethyl ether (2 × 10 mL each) to yield a mixture of **3a**, **3b**, and **3d** (1.80 g). The characteristic peaks in the $^{13}C\{^1H\}$ NMR spectrum of **3d** are δ 93.5 (C_5H_5), 91.1 (*C*Ph), 51.7 (*C*Ph), and 51.3 (*C*Ph).

(η^5-Cyclopentadienyl)(η^3-triphenylcyclopropenyl)diiodoruthenium(IV) (3c). The mixture of **3a**, **3b**, and **3d**, prepared as above was allowed to react with excess KI in methanol (50 mL). After 12 h a brown solid was removed by filtration and washed with diethyl ether (2 × 15 mL) to yield **3c** (1.2 g, 1.8 mmol, 88%): mp 160 °C; ^{1}H NMR ($CDCl_3$) δ 8.02 (m, br, 4H, Ph), 7.94 (m, br, 2H, Ph), 7.48 (m, br, 6H, Ph), 7.38 (m, br, 3H, Ph), 5.30 (s, 5H, C_5H_5); $^{13}C\{^1H\}$ NMR ($CDCl_3$) δ 134.1, 131.6, 130.2, 129.8, 129.3, 129.1, 126.9, 125.6 (Ph), 91.8 (C_5H_5), 80.2 (1C, *C*Ph), 46.0 (2C, *C*Ph). Anal. Calcd for $C_{26}H_{20}I_2Ru$: C, 45.43; H, 2.94; I, 36.93. Found: C, 45.81; H, 2.97; I, 37.02.

(η^5-Pentamethylcyclopentadienyl)(η^3-triphenylcyclopropenyl)dichlororuthenium(IV) (3e). To THF (6 mL) was added [RuCp*(μ_3-Cl)]$_4$ (0.10 g, 0.096 mmol) and triphenylcyclopropenyl chloride (0.11 g, 0.37 mmol). The mixture was allowed to stir for 4 days, after which time the mixture had turned deep red. The solvent was removed via cannula filtration and the brown residue was washed with THF (2 × 5 mL) and petroleum ether giving orange-red **3e** (0.15 g, 75%): dec 175–178 °C; ^{1}H NMR ($CDCl_3$) δ 8.10 (m, br, 4H, Ph), 7.86 (m, br, 2H, Ph), 7.41 (m, br, 6H, Ph), 7.26 (m, br, 3H, Ph), 1.34 (s, 5H, C_5Me_5); $^{13}C\{^1H\}$ NMR ($CDCl_3$) δ 134.1, 131.1, 130.4, 129.1, 128.8, 128.5, 126.8, (Ph), 102.3 (*C*$_5$Me$_5$), 90.1 (1C, *C*Ph), 50.2 (2C, *C*Ph), 9.1 ($C_5(CH_3)_5$). Anal. Calcd for $C_{31}H_{30}Cl_2Ru$: C, 64.80; H, 5.26. Found: C, 65.01; H, 5.62.

(η^5-Pentamethylcyclopentadienyl)(η^3-triphenylcyclopropenyl)dibromoruthenium(IV) (3f). A red THF (12 mL) solution of [RuCp*(μ_3-Cl)]$_4$ (0.159 g, 0.586 mmol), triphenylcyclopropenyl bromide (0.203 g, 0.586 mmol), and LiBr (0.44 g, 5.1 mmol) was stirred overnight. The solvent was then removed under reduced pressure, and the product was extracted with CH_2Cl_2 and filtered through Celite. Removal of the CH_2Cl_2 under reduced pressure gave **3f** (0.383 g, 0.577 mmol, 98.5%). **3f** may be purified by chromatography on silica gel, eluting with petroleum ether followed by CH_2Cl_2. dec 209–212 °C; ^{1}H NMR ($CDCl_3$) δ 8.10 (m, br, 4H, Ph), 7.86 (m, br, 2H, Ph), 7.41 (m, br, 6H, Ph), 7.26 (m, br, 3H, Ph), 1.34 (s, 15H, C_5Me_5); $^{13}C\{^1H\}$ NMR ($CDCl_3$) δ 133.9, 131.4, 130.5, 128.9, 128.7, 128.6, 127.6, 126.7 (Ph), 102.0 (*C*$_5$Me$_5$), 85.8 (1C, *C*Ph), 47.7 (2C, *C*Ph), 10.0 ($C_5(CH_3)_5$). Anal. Calcd for $C_{31}H_{30}Br_2Ru$: C, 56.12; H, 4.56. Found: C, 55.73; H, 4.61.

(η^5-Pentamethylcyclopentadienyl)(η^3-triphenylcyclopropenyl)diiodoruthenium(IV) (3g). A refluxing red solution of [RuCp*(η^3-C_3Ph_3)Cl_2] (**3e**) (0.471 g, 0.710 mmol) in CH_2Cl_2 (20 mL) was treated with aqueous HI (1.16 mL, 57%, 8.5 mmol). The solution turned darker orange and was stirred for 1 h. The solution was allowed to cool, and distilled degassed water (10 mL) was added to give a pale orange gray aqueous layer and a black organic layer. The organic layer was separated and the solvent was removed under reduced pressure, affording the product as a deep red solid (0.540 g, 0.710 mmol, 100%). Recrystallization from CH_2Cl_2/petroleum ether gave black needles: dec 154–157 °C, ^{1}H NMR ($CDCl_3$) δ 8.15 (m, br, 4H, Ph), 7.89 (m, br, 2H, Ph), 7.41 (m, br, 6H, Ph), 7.29 (m, br, 3H, Ph), 1.78 (s, 15H, C_5Me_5); $^{13}C\{^1H\}$ NMR ($CDCl_3$) δ 133.6, 131.6, 130.6, 128.9, 128.6, 128.5, 128.4 (Ph), 101.4 (*C*$_5$Me$_5$), 99.0 (1C, *C*Ph), 43.7 (2C, *C*Ph), 11.8 ($C_5(CH_3)_5$). Anal. Calcd for $C_{31}H_{30}I_2Ru$: C, 49.16; H, 3.99. Found: C, 48.96; H, 4.07.

(η^5-Cyclopentadienyl)(η^3-trimethylcyclopropenyl)dichlororuthenium(IV) (4a). [RuCp(η^4-COD)Cl] (1.34 g, 4.32 mmol), [C_3Me_3][BF_4] (0.92 g, 5.5 mmol), and LiCl (0.72 g, 17 mmol) were dissolved in THF (25 mL). The solution turned deep red and became progressively more red-black over the next several hours. It was allowed to stir overnight. The resulting orange precipitate was separated via filter cannula giving the product as an orange solid. (1.22 g, 3.84 mmol, 89%). Recrystallization from CH_2Cl_2 afforded orange needles: dec 130 °C; ^{1}H NMR ($CDCl_3$, 21 °C) δ 5.20 (s, 5H, C_5H_5), 2.38 (s, br, 9H, CH_3); $^{13}C\{^1H\}$ NMR ($CDCl_3$, −30 °C) δ 101.2 (1C, *C*$_3$Me$_3$), 90.3 (C_5H_5), 59.9 (2C, *C*$_3$Me$_3$), 10.6 (2C, CH_3) 8.5 (1C, CH_3). Anal. Calcd for $C_{11}H_{14}Cl_2Ru$: C, 41.52; H, 4.43. Found: C, 41.17; H, 4.54.

(η^5-Cyclopentadienyl)(η^3-trimethylcyclopropenyl)dibromoruthenium(IV) (4b). To a refluxing orange solution of [RuCp(η^3-C_3Me_3)Cl_2] (0.060 g, 0.19 mmol) in CH_2Cl_2 (10 mL) was added aqueous HBr (0.34 mL, 48%, 3.0 mmol). The solution turned dark red-black at once and was stirred for 1 h. After cooling to room temperature, distilled degassed water (10 mL) was added to give a pale orange-gray aqueous layer and a red-black organic layer. The organic layer was separated and the solvent was removed under reduced pressure to afford **4b** as a deep red-orange solid (0.075 g, 0.18 mmol, 96%). Recrystallization from CH_2Cl_2 afforded orange-red needles: dec 148 °C; ^{1}H NMR ($CDCl_3$, 21 °C) δ 5.26 (s, 5H, C_5H_5), 2.68 (s, br, 6H, CH_3), 2.34 (s, br, 3H, CH_3); $^{13}C\{^1H\}$ NMR ($CDCl_3$, −30 °C) δ 96.8 (1C, *C*$_3$Me$_3$), 89.9 (C_5H_5), 57.4 (2C, *C*$_3$Me$_3$), 10.6 (2C, CH_3), 1.0 (1C, CH_3). Anal. Calcd for $C_{11}H_{14}Br_2Ru$: C, 32.45; H, 3.47. Found: C, 32.34; H, 3.51.

(η^5-Cyclopentadienyl)(η^3-trimethylcyclopropenyl)diiodoruthenium(IV) (4c). To a refluxing orange solution of [RuCp(η^3-C_3Me_3)Cl_2] (0.15 g, 0.47 mmol) in CH_2Cl_2 (10 mL) was added aqueous HI (0.75 mL, 57%, 5.6 mmol). The solution turned dark red-black at once and was stirred for 1 h. The solution was cooled, and then distilled degassed water (10 mL) was added. This gave a pale orange-gray aqueous layer and a red-black organic layer. The organic layer was separated and the solvent removed under reduced pressure, giving the product as a deep red solid (0.19 g, 0.38 mmol, 81%). Recrystallization from CH_2Cl_2 afforded red-orange needles: dec 146 °C; ^{1}H NMR ($CDCl_3$, 21 °C) δ 5.33 (s, 5H, C_5H_5), 2.92 (s, br, 6H, CH_3), 2.34 (s, br, 3H, CH_3); $^{13}C\{^1H\}$ NMR ($CDCl_3$, −30 °C) δ 88.9 (C_5H_5), 88.1 (1C, *C*$_3$Me$_3$), 53.1 (2C, *C*$_3$Me$_3$), 10.9 (2C, CH_3), 1.0 (1C, CH_3). Anal. Calcd for $C_{11}H_{14}I_2Ru$: C, 26.37; H, 2.82. Found: C, 26.36; H, 2.97.

(η^5-Pentamethylcyclopentadienyl)(η^3-trimethylcyclopro-

penyl)dichlororuthenium(IV) (4d). [RuCp*(μ_3-Cl)]$_4$ (0.68 g, 2.5 mmol), [C_3Me_3][BF_4] (0.42 g, 2.5 mmol), and LiCl (0.37 g, 8.8 mmol) were dissolved in THF (25 mL). The solution turned dark orange-black and was stirred for 19.5 h. An orange precipitate formed and was isolated via filter cannula affording the product as an orange solid (0.94 g, 2.4 mmol, 96%): dec 151 °C; ^{1}H NMR ($CDCl_3$, 21 °C) δ 2.16 (s, br, 9H, CH_3), 1.64 (s, 15H, C_5Me_5); $^{13}C\{^1H\}$ NMR ($CDCl_3$, −30 °C) δ 101.1 (C_5Me_5), 96.8 (1C, C_3Me_3), 55.9 (2C, C_3Me_3), 9.6 (1C, CH_3), 9.5 ($C_5(CH_3)_5$), 8.2 (2C, CH_3). Anal. Calcd for $C_{16}H_{24}Cl_2Ru$: C, 49.49; H, 6.23. Found: C, 49.23; H, 6.11.

(η^5-Pentamethylcyclopentadienyl)(η^3-trimethylcyclopropenyl)dibromoruthenium(IV) (4e). A refluxing orange solution of [RuCp(η^3-C_3Me_3)Cl_2] (0.27 g, 0.70 mmol) in CH_2Cl_2 (10 mL) was treated with aqueous HBr (1.26 mL, 48%, 11.1 mmol). The solution turned dark red-black at once and was stirred for 1 h. The solution was cooled, and then distilled degassed water (10 mL) was added. This gave a pale orange-gray aqueous layer and a red-black organic layer. The organic layer was separated and the solvent was removed under reduced pressure, giving deep orange **4e** (0.26 g, 0.55 mmol, 78%). Recrystallization from CH_2Cl_2 gave orange-red needles: dec 151–153 °C; ^{1}H NMR ($CDCl_3$) δ 2.62 (s, br, 6H, CH_3), 2.09 (s, br, 3H, CH_3), 1.76 (s, 5H, C_5H_5); $^{13}C\{^1H\}$ NMR ($CDCl_3$, −30 °C) δ 99.8 (C_5Me_5), 93.0 (1C, C_3Me_3), 53.7 (2C, C_3Me_3), 12.2 (1C, CH_3), 10.1 ($C_5(CH_3)_5$), 8.3 (2C, CH_3). Anal. Calcd for $C_{16}H_{24}Br_2Ru$: C, 40.27; H, 5.07. Found: C, 40.19; H, 5.00.

(η^5-Pentamethylcyclopentadienyl)(η^3-trimethylcyclopropenyl)diiodoruthenium(IV) (4f). To a refluxing orange solution of [RuCp(η^3-C_3Me_3)Cl_2] (0.22 g, 0.57 mmol) in CH_2Cl_2 (10 mL) was added aqueous HI (0.91 mL, 57%, 6.8 mmol). The solution turned darker orange and was stirred for 1 h. The solution was cooled, and then distilled degassed water (10 mL) was added. This gave a pale orange-gray aqueous layer and a dark orange organic layer. The organic layer was separated and the solvent was removed under reduced pressure, affording a deep orange-black solid (0.31 g). Recrystallization from CH_2Cl_2 gave black needles: ^{1}H NMR ($CDCl_3$) δ 2.86 (s, br, 6H, CH_3), 2.08 (s, br, 3H, CH_3), 1.97 (s, 15H, C_5H_5, this tentative assignment is based on the Cl_2 and Br_2 analogues which contain C_5H_5 resonances at δ 1.64 and 1.76 respectively), 1.68 (not assigned, but see text).

Acknowledgment. We are grateful to the National Science Foundation and to the donors of the Petroleum Research Fund, administered by the American Chemical Society, for generous support of our research. A generous loan of ruthenium salts from Johnson Matthey Aesar/Alfa is also gratefully acknowledged.

Supplementary Material Available: Appendix A, a listing of molecular geometries used in extended Hückel calculations (2 pages). Ordering information is given on any current masthead page.

OM920811E